-RESEARCH PAPER-

International Journal of Mining and Geo-Engineering

IJMGE

IJMGE 58-2 (2024) 191-201

DOI: 10.22059/IJMGE.2024.351410.595002

Evaluation of compressive capacity of the helical pile resting in the cohesionless soil

Hitesh Rahi [a], Jitendra Singh Yadav [b,*], Shaik Hussain [c]

[a] *Department of Civil Engineering, National Institute of Technology Hamirpur, Himachal Pradesh, India.*

[b] *Department of Civil Engineering, National Institute of Technology Kurukshetra, Haryana, India.*

[c] *Trenchless Technology Center, Louisiana Tech University, United States.*

Article History:

Received: 20 November 2022.

Revised: 25 October 2023.

Accepted: 13 January 2024.

ABSTRACT

Current research deals with the numerical investigation of the behavior of helical piles resting in cohesionless soil subjected to compressive load. The effect of the diameter of pile shaft (D_S), the diameter of the helical plate (D_h), the depth of the pile (H), the inter-helical spacing ratio (S/D_h) the number of helix (m), and the type of sand on the load-displacement behaviour of helical pile was evaluated. The numerically determined compression capacity of the helical pile was compared with the existing theories. Apart from this, the artificial neural network technique was employed on the obtained results to develop the model equation. An increase in the compression capacity of single and double helical pile was observed with an increase in the pile depth, the friction angle of sand, and the diameter of pile shaft. For double helical pile, the optimum inter-helix spacing ratio was found to be 3.

Keywords: *Helical pile, Compression capacity, Failure mechanism, Finite-element analysis.*

Notations

H: Depth of pile
Ds: Diameter of shaft
ts: Thickness of shaft
Dh: Diameter of helix
th: Thickness of helix
m: Number of helices
γ: Unit weight
ϙ: Unit Density
ϕ: Internal Friction angle
E: Elastic modulus
μ: Poisson's ratio
ψ: Dilation Angle
Nq': Bearing capacity Factor
β: Reduction Factor
n: Number of helices except end helix
An: Area of nth helical plate except end helix
Aend: Surface area of bottom helical plate
fs: Shear stress along the surface of pile shaft
d: Diameter of a circle circumscribed around the shaft
Kh: Lateral earth pressure coefficient for helical pile
He: Pile depth above the uppermost helix
S: Distance between helical plates
CSF: Cylindrical shear failure
IBF: Individual bearing failure

1. Introduction

Helical pile consists of a central shaft alongside one or more helical plates (called helix) manufactured from high-strength steel. Helical bearing plates are welded to the pile shaft in accordance with the intended ground condition. The central shaft is a hollow, circular steel pipe section which is inserted into the ground by transmitting torque during installation. Helical pile can offer resistance against axial and lateral forces and overturning moments which provide stability to the structure rested on it. Helical pile foundation can be installed in confined spaces with minimal soil disruption. It can be installed rapidly and sustain load immediately.

During the installation of helical piles, the stiff subsoil condition can distort or tear the helical pile and its welds which may lead to an increase in the installation resistance, uneven loading, welding integrity, and bucking of the helical pile. More resistance is provided during installation by stiff sublayers. The stiff sublayer's resistance can impose a sizable torque and axial force on the helical piles as they are rotated into the earth. The piles may twist or distort if they are not built to handle such tremendous stresses. Uneven stress on the helical plates may result from variations in the stiffness of various sublayers. Unbalanced loading may happen if one part of the pile is in a stiff sublayer while another is in a softer sublayer. The pile may experience bending or twisting forces as a result of this uneven loading, leading to deformation. A crucial component of helical pile building is the welding that connects the helical plates to the central steel shaft. When installing the piles, stiff sublayers may impose too much twisting and torsional load on them. The welds may weaken or even rip, resulting in structural failure, if the welding is not done well or if the design does not take these stresses into consideration. The helical piles may buckle due to stiff sublayers. When a pile or other thin structural component collapses from too much compressive force, it buckles. If the applied axial loads are not evenly distributed or if the pile is not built to withstand buckling under specified circumstances, stiff sublayers may cause the pile to buckle.

Before developing helical pile foundations, engineers must thoroughly assess the soil conditions in order to reduce these problems. Understanding the soil profile and the changes in stiffness at different depths requires site-specific geotechnical studies. It is crucial to use suitable pile design, taking into account the expected loads and soil characteristics. Additionally, to reduce the dangers connected with

* Corresponding author. *E-mail address:* : jsyadav@nitkkr.ac.in (J. Singh Yadav).

installing helical piles in heterogeneous sublayers, construction techniques that can adapt to changing soil conditions should be employed.

In the past, many researchers have analyzed the behavior of helical pile resting in different type of soil through laboratory test, field test, and numerical analysis. Rao et al. [1] evaluated the performance of helical pile resting in cohesive soil and concluded that the ratio of spacing of helical plate to the diameter of the plates should be kept between 1.0 and 1.5. The decrement in the moisture contents led to a significant increment in the bearing capacity of the piles. Furthermore, Rao et al. [2] investigated that the compression capacity of helical anchor increases with the increment of embedment depth. At spacing ratios higher than 1.5-2.0 for helical plates, the individual plate bearing method underestimates the capacities in soft marine clays. For multi-helix helical pile, two types of failure mechanisms were considered: individual bearing failure (IBF) and cylindrical shear failure (CSF) [1] [3] [4].

Lutenegger [5] performed a field investigation and reported that for a multi-helical screw pile in clay with an inter-helical spacing ratio of 3, there was no definite transition from CSF to IBF. Sprince and Pakrastins [6] concluded that the diameter size of the bearing plate affects the load-bearing capacity of a helical screw pile, but not equally in all soils. Lutenegger [7] found that for a multi-helix screw pile in sand with a spacing ratio of 3, the failure mechanism changes from CSF to IBF. The efficiency of multi-helix anchors in sand was found to decrease with the number of helical plates along the shaft. Nabizadeh and Choobbasti [8] concluded from field work on cohesionless soil that for an inter-helical spacing ratio of 1.5, the CSF was more likely to occurre.

Salhi et al., [9] investigated that for the cohesionless soil, the bottom helix developed a greater resistance than the other helices, irrespective of inter-helical spacing ratio (S/Dh). Elsherbiny and El Naggar [4] found that the primary mechanism of load transmission was through IBF. However, as the spacing between the helical plates reduces, the compression capacity also reduces. Knappett et al., [10] concluded that the torque during the installation and compression capacity of screw pile increases with the relative density of sand. Sırsıkar [11] reported a significant increment in the compression capacity with an increase in the inter-helical spacing ratio of helical pile resting in sand. Also, with the increase in the spacing ratio, load transfers from the end helix to the middle and uppermost helix. George et al., [12] documented that the shaft diameter plays an insignificant role compared to that of the helix diameter in the evaluation of ultimate axial load carrying capacities. Nowkandeh and Choobbasti [13] numerically evaluated the performance of helical pile resting in sandy and clayey soil and showed that the optimum inter-helical spacing between helices in sandy and clayey soil was $3D_h$ and $2D_h$, respectively. However, furthermore investigation was recommended to understand the behaviour of helical pile in soil. The efforts made by the investigators in the past are quite insignificant to understand the effect of the diameter of pile shaft, the diameter of helical plate, the depth of pile, the inter-helical spacing ratio, and the number of helixes on the behaviour of helical pile resting in different types of sand. Dev et al. [14] reported an increment in the uplift capacity of helical with increases in ϕ, n, H, and S/D_p. However, a decrease in Q_u for single and double-helical piles was noted with an increase in the D_p/D_s ratio. Nowkandeh and Ashtiani [15] examined the behaviour of cushioned helical-piled raft systems to mitigate hazards associated with normal faulting. Mehrabani et al. [16] evaluated the effect of angle, length, and the number of micropiles on their pull-out force through field test. The maximum pull-out force was recorded at the installation angle of 30 degrees to the vertical axis. Alipour et al. [17] reported that length and number of micropiles have the greatest effect on the control of the deformation field and settlement of the structure.

The current study intends to evaluate the behavior of single and double helix piles resting in loose sand ($\phi = 25°$), medium sand ($\phi = 33°$), and dense sand ($\phi = 40°$) subjected to compressive load. The effects of the diameter of the pile shaft, the diameter of the helical plate, the depth of the pile, the inter-helical spacing ratio, and the number of helixes on the load-displacement behavior of helical pile have been assessed. Furthermore, the numerical results were compared with various theories purposed by different investigators. The compression capacity of the helical pile was compared with that of under-reamed and conventional concrete pile.

2. Problem Outlines and Modelling

The soil was modeled as a solid three-dimensional (3D) cylinder in shape having deformable type with an extrusion base feature. The helical pile was placed at the center of the numerical model, aligned parallel to the z-direction of the cylindrical soil model. Fig.1 shows the line diagram of a single helical pile under compressive load. The boundaries of the numerical model extended a distance more than twenty times the helix diameter and the soil depth beneath the pile bottom was ten times the helix diameter. This was done to minimize boundary effects on the numerical model. Table 1 shows the different parameters of the helical pile varied in this investigation.

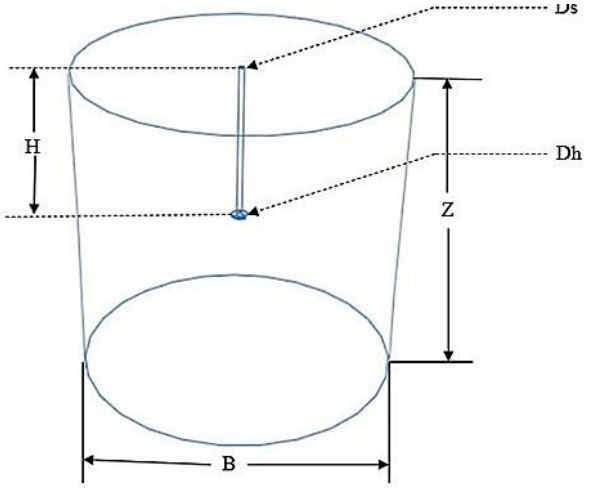

Fig. 1 Line Diagram of the numerical model.

Table 1. Parameter varied for the numerical analysis.

Description	Spacing Ratio (S/D_h)	Pile Depth (m)	D_h/Ds ratio	Friction Angle ϕ (°)
Single helix		6	2, 3, 4	25, 33, 40
		8	2, 3, 4	25, 33 ,40
Double helix	**1.5**	6	2, 3, 4	25, 33, 40
		8	2, 3, 4	25, 33, 40
	2	6	2, 3, 4	25, 33, 40
		8	2, 3, 4	25, 33, 40
	3	6	2, 3 ,4	25, 33, 40
		8	2, 3, 4	25, 33, 40

2.1. Pile Characteristic

The pile was modeled as a hollow circular shaft having deformable type with an extrusion base feature. The helical plate was modeled as a three-dimensional helical in shape with a revolution base feature. The geometry of the helical pile created using ABAQUS is displayed in Fig. 2 (a). Table 2 displays the material properties of the helical pile. The depth of the helical pile was taken as 6 m and 8 m. The diameter of helix was taken as 610 mm [13]. The diameter of the pile shaft was taken according to the Dh/Ds ratio (2, 3, and 4). In the case of a double helix, the spacing between helical plate depends on the diameter of the helix. Thus, three inter-helical spacing ratios were considered (as 1.5, 2, and 3). For the numerical analysis, one variable was altered while others were kept constant to study the effect of each parameter.

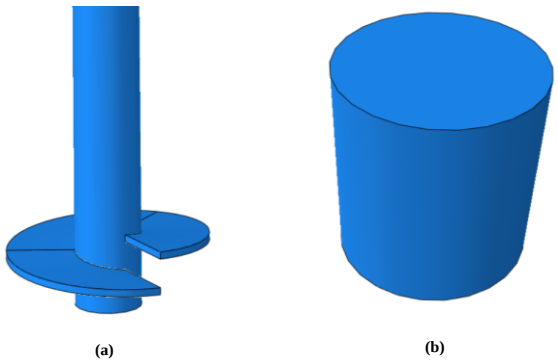

Fig. 2 Part of helical pile (a) and soil (b) using Abaqus.

Table 2. The properties of the helical pile used for numerical modelling [13].

Properties	Values
Mass Density, ϱ	7850 kg/m³
Poisson's Ratio, μ	0.3
Modulus of Elasticity, E	200 GPa

2.2. Soil Parameters

In this study, the soil was modeled as an elasto-plastic material. The Mohr-Coulomb model was chosen to describe the failure criterion. The geometry of soil created using ABAQUS is shown in Fig. 2 (b). Three types of sandy soil i.e., loose, medium, and dense sandy soil were considered for this investigation. Table 3 displays the physical properties of cohesionless soil used in this work.

Table 3. Properties of soil used for numerical modelling [13].

Soil Type (Sand)	Friction Angle (°)	Unit Weight (kN/m³)	Modulus of Elasticity, E (MPa)	Poisson's Ratio	Dilation Angle (°)	Mass Density (kg/m³)
Loose	25	16	10	0.3	0	1631
Medium	33	18	30	0.3	3	1835
Dense	40	20	50	0.3	10	2039

The parameters varied for analysis are the unit density of the soil (ϱ), internal friction angle (ϕ), modulus of elasticity (E) and Dilation angle (ψ). The values of unit density taken for analysis were 1631 kg/m³, 1835 kg/m³, and 2039 kg/m³ corresponding to the values of the friction angles 25°, 33°, and 40°, respectively. The dilation angle was calculated using (ϕ -30°) for modelling, as per Szypcio and Dołżyk, [14] and taken as 0, 3, and 10. The values of the elasticity modulus (E) were taken as 10 MPa, 16 MPa, and 50 MPa, respectively.

The interface friction angle or skin friction between pile and soil is defined by the tangential behavior as a contact property using the penalty-type Coulomb's Frictional model. The value of the friction coefficient was calculated as tan(0.7ϕ) as per Stas and Kulhawy [15]. Therefore, the friction coefficients between the soil and pile for loose, medium, and dense sandy soil were taken as 0.31, 0.42, and 0.53, respectively. The tie constraint was used to provide an interaction between the shaft and helix using surface-to-surface discretization method.

2.3. Meshing and Boundary condition

A linear brick element with 8-node reduced-integration (C3D8R) was used for meshing the soil part, except for the geometric region where the helix was present. Thus, a 10-node modified quadratic tetrahedron meshing (C3D10M) was used for that geometric region. Fig. 3 (a) & 3 (b) represent the meshing used for the numerical model. For the helical pile, an eight-node linear brick, reduced integration (C3D8R), was used as an element shape for meshing as shown in Fig. 3 (c) & 3 (d). The mesh refinement was used to obtain accurate and precise results. The meshing of helical pile and soil at center was finer and increased gradually towards the outer side of the soil model. For the basic meshing, the number of elements used for soil part and helical pile were 50403 and 10000, respectively.

Boundary condition applied at the soil bottom was restrained in every direction ($U_X = U_Y = U_Z = 0$). On the side, displacement was restrained in the X and Y directions, while the Z direction was free to move ($U_X = U_Y = 0$). The model's top face was supposed to be free in every direction. The displacement of 0.30 m was applied at the reference point in the dynamic explicit model. The reference point was restricted in all directions ($U_X = U_Y = U_Z = U_{R1} = U_{R2} = U_{R3} = 0$). Fig. 4 represents the loading and boundary conditions of the model.

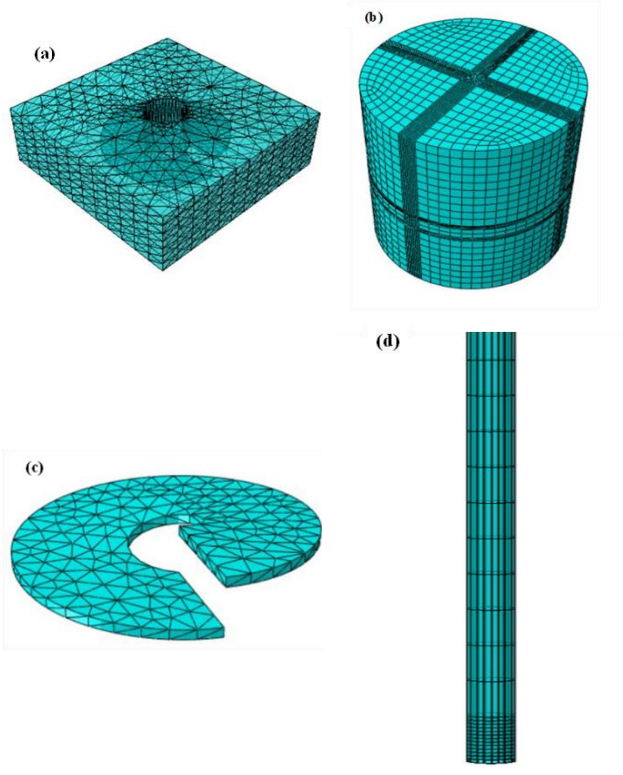

Fig. 3 Meshing (a) internal part, (b) soil, (c) helical plate and (d) pile shaft.

2.4. Failure criterion considered

The Federal Highway Administration (FHWA) criterion [16] suggests that for drilled shaft, the axial capacity can be considered as the load value of equivalent to the settlement of 5% of the helical blade diameter. As per, Elsherbiny and El Naggar [4] the ultimate compression capacity of a helical pile depends upon the diameter of helix. For the value of helix diameter (D_h) greater than 600 mm and less

than 305 mm, the load corresponding to displacement of 5% and 10% of D_h were used as failure criterion. This method was used in the numerical model to find the compression capacity of each helical pile. For helix having diameter 610 mm, the displacement of 30 mm was given in the dynamic explicit loading module for modelling.

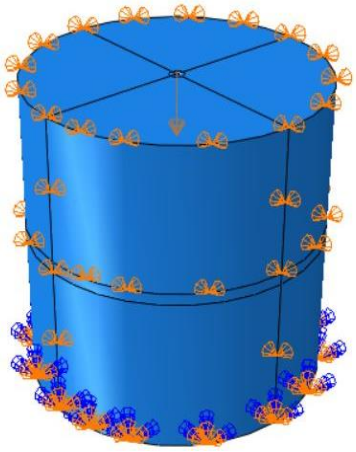

Fig. 4 Boundary Conditions applied in ABAQUS.

3. Model validation

The results obtained by Elsherbiny and El Naggar [4] on full-scale pile load test on helical pile were used to validate the model. Elsherbiny and El Naggar [4] selected two sites: Site (A) and Site (B) had a cohesionless and clayey soil profile located in northern Alberta, and northern Ontario, Canada, respectively. At side (A), the shape of the pile shaft was cylindrical having one helix. Site (A) had two test piles named PA-1 and PA-2. At site (A), the depth of the helical pile was 5.5 m, and a shaft with a diameter of 273 mm and thickness of 9.3 mm was installed. The maximum compression load taken by this pile after three days was 210 kN. The maximum settlement was found to be varied from 9 to 12 mm.

A finite element-based numerical model was also created by Elsherbiny and El Naggar [4] using ABAQUS to replicate field testing data. The soil and steel properties taken by Elsherbiny and El Naggar (2013) were used for the numerical validation. The load-displacement curve obtained from the compression test at Site (A) was compared with the load-settlement curve obtained from the present numerical model, as represented in Fig. 5. The results obtained through numerical investigation were found to be similar to the field test results reported by Elsherbiny and El Naggar [4]. Fig. 5 shows that the compression capacity obtained by Elsherbiny and El Naggar [4] from field testing was 210 kN, whereas the numerical capacity from software analysis was 200 kN. The percentage variation in the numerical capacity obtained from software analysis was less than 5% compared to the field capacity.

4. Result and Discussion

The numerical modelling was carried to determine the effect of parameters such as the diameter of pile shaft (D_S), the diameter of helical plate (D_h), the depth of pile (H), the inter-helix spacing ratio, and the number of helixes on the load-displacement behavior of the helical pile resting in loose, medium, and dense sandy soil. This section discusses the effect of all these parameters on the compression capacity of single and double helical pile.

4.1. Single helical pile

4.1.1. The impact of sand attributes

Fig. 6 (a) and (b) reveal the load-displacement behavior of the helical pile having pile depth of 6 m and 8 m resting in different sandy soils at D_h/D_S ratio of 2. The end bearing of the helix is significantly influenced by physical properties of the soil, such as the friction angle, Young's modulus, specific density, and cohesion. It can be concluded from Fig. 6 (a) that as the internal friction of the soil increases, the compression capacity of the helical pile enhanced significantly. For loose (ϕ = 25°), medium (ϕ = 33°), and dense sand (ϕ = 40°), the values of the compression capacity for 6 m pile depth were 120 kN, 255 kN, and 678 kN, respectively. Similarly, for a pile depth of 8 m, the compression capacity were 185 kN, 410 kN, and 950 kN, respectively. It is obvious that an increase in the internal friction angle of the sandy soil leads to increased end resistance. Perko and Wiley [17] suggested Eq. (i) to determine the compression capacity of the helical pile failed under IBF. The first and second terms of Eq (i) indicate the end bearing of helixes in sandy soil, and mobilized shear forces around the pile shaft is represented by the third term of the equation.

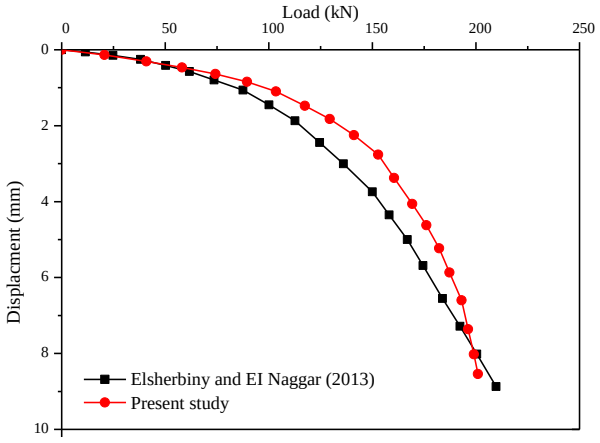

Fig. 5. Load vs Displacement of pile tested in the cohesionless soil and the numerically calibrated model using FEM.

4.1.2. The impact of Pile Depth(H)

The load-displacement behavior of single helical piles with different lengths in medium sand at D_h/D_S = 3 is shown in Fig. 7. The obtained load-displacement curve exhibited an initial linear portion followed by a non-linear term. With the increase in the helical pile depth, the compression capacity also increases. For medium sandy soil at D_h/D_S = 3, the load capacity obtained for 6 m and 8 m pile depth was 252.65 kN and 346.92 kN, respectively. This increase in the compression capacity with the increase in pile depth may be accredited to an increase in the shaft resistance. This finding confirms that the end bearing resistance of helixes in cohesionless soil is significantly dependent on their embedded pile depth.

4.1.3. The effect of Dh/DS on compression capacity

The load-displacement behavior of helical pile resting in medium sandy soil at different D_h/D_S ratios having 6 m and 8 m depths are shown in Fig 8 (a) and (b). In this study, the diameter of helix was kept constant at 610 mm and the diameter value of the shaft varied for D_h/D_S ratios of 2, 3, and 4. With the increase in D_h/D_S ratio, the diameter of the shaft reduces. For instance, at D_h/D_S = 2 for a pile depth of 6 m, the compression capacity was 255 kN which reduced to 252.65 kN, and 239.88 kN for D_h/D_S = 3 and 4, respectively. Similarly, for 8 m pile length, the compression capacity was 410 kN at D_h/D_S = 2, declining to 346.92 kN and 305.14 kN for D_h/D_S = 3 and 4, respectively. It was noticed that the gradient of load-displacement plots was initially linear, increased steeply with the increment in the diameter of shaft. The stiffness behavior of the shaft is governed by the diameter of the pile shaft. The reduction in the compression capacity due to the increase in D_h/D_S ratio may be due to the availability of the smaller surface area along the pile shaft to interact with the surrounding soil.

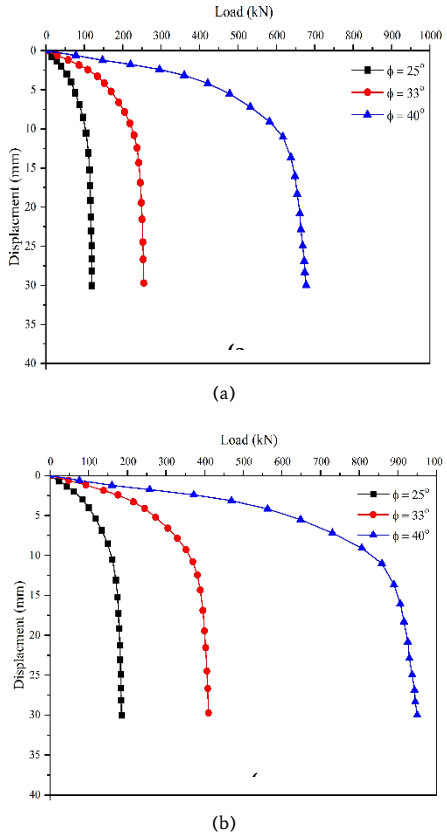

Fig. 6. Load-displacement curves of the single helical pile resting in loose, medium, and dense sandy soil having (a) 6 m and (b) 8 m pile depths (Dh/DS = 2).

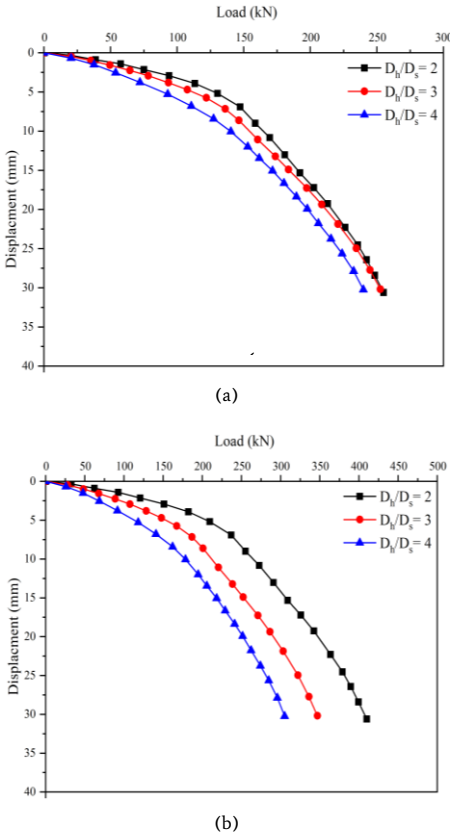

Fig. 8 Load-displacement curves of the single helical pile resting in medium sandy soil for different Dh/Ds ratios (L = 6 m and 8 m).

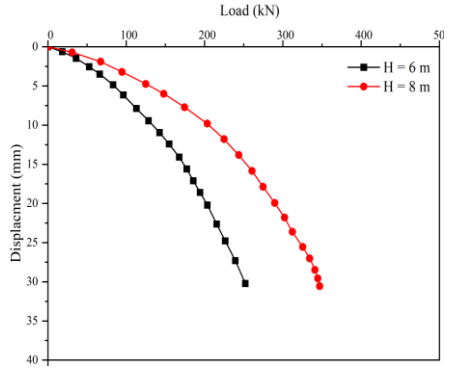

Fig. 7 Load-displacement curves of the single helical pile for different pile depths in medium sandy soil having Dh/Ds=3.

4.1.4. Displacement contour

Vertical displacement contours of medium sand having different D_h/D_S ratios of 2, 3 and 4 and pile lengths of 6 m and 8 m are illustrated in Figs. 9 and 10, respectively. For all the cases shown in Figs. 9 and 10, it was found that the displacement of soil was contained around the pile tips and helix. The individual bearing failure mechanism was seen in all cases. Furthermore, it was observed that with a decrease in the diameter of single helical pile, the magnitude of the displacement under the helix and at the tip of the pile increased. This decrease in displacement magnitude with the increase in diameter of single helical pile may be responsible for the behavior discussed in 4.1.3.

4.1.5. Theoretical Capacity for single helical pile

The Pile compression capacity is calculated by considering the failure mechanism of a helical pile in sandy soil. Mitsch and Clemence [18], Elsherbiny and El Naggar [4], Perko and Wiley [17], and Nowkandeh and Choobbasti [13] suggested two methods to determine the ultimate compression capacity of the pile: (1) the ultimate compression capacity based on IBF, and (2) the ultimate compression capacity based on the CSF. The ultimate compressive capacity of helical pile for IBF is calculated as:

$$P_{individual} = \sum_n [2Dh\gamma(Nq' - 1)An] + 2Dh\gamma(Nq' - 1)Aend + fsH\pi d \quad \text{(i)}$$

Where,

$$Nq' = [e^{\pi \tan\phi} \tan^2(45+\phi/2)][1+\tan\phi]\,[1+\pi\tan\phi][1-\sin\phi]^2 \quad \text{(ii) [17]}$$

$$Fs = 0.66\gamma K_h\,(H/2)\,\tan\phi \quad \text{(iii)}$$

$$Kh = 0.09e^{0.08\phi} \quad \text{(iv) [18]}$$

The first term of Eq. (i) calculates the end bearing of each helix except the bottom helix. The second term calculates the end bearing of the bottom helix. The third one considers the shear force mobilized around the pile shaft. Perko and Wiley[17] proposed that the bearing pressure became critical at some depth of the helical pile, and it was equal to twice the helix diameter (the first and second terms of Eq. (i). For loose sand, it was expected that the installation of helical pile could increase the friction angle. However, for safe design, the average shaft shear stress was not increased. For a pile in medium and dense sand, a reduction factor of 0.66 was applied to the average shear stress along the shaft (f_s) [13][13][13][13][13][13][13][13][12][12][12][13][12][12][12][12](Nowkandeh and Choobbasti, 2021). For medium dense sand, the compression capacity based on individual bearing failure can be calculated as:

$\phi = 30°$; $D_h = 0.61$ m; $\gamma = 17$ kN/m^3; $N_q' = 20.42$; $A_n = 0$ m^2; $A_{end} = 0.293$ m^2; $n = 0$; $H = 5.5$ m; $d = 0.273$ m; $K_h = 0.99$; $f_s = 17.67$

$$P_{individual} = 0 + 118.01 + 83.35 = 201.36 \text{ kN} \quad \text{(v)}$$

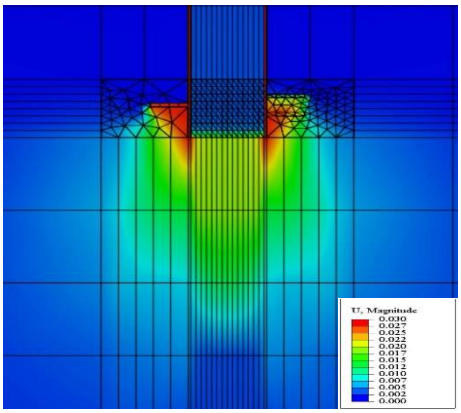

(a)

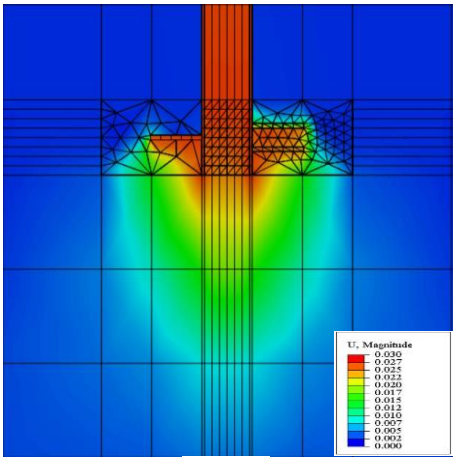

(b)

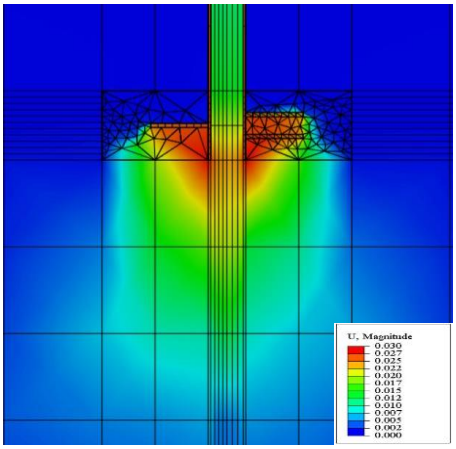

(c)

Fig. 9 Vertical Displacement Contours of the single helical piles resting in medium sandy soil having different Dh/Ds ratios for 6m Pile Length: (a) Dh/Ds=2 (b) Dh/Ds=3 (c) Dh/Ds=4.

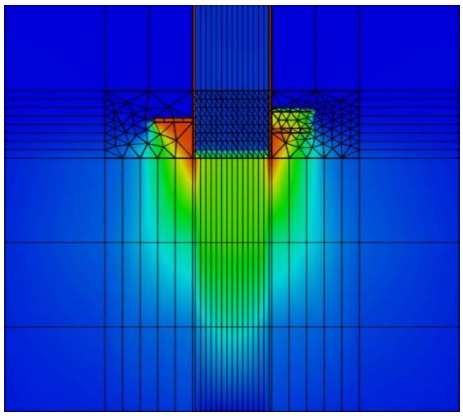

(a)

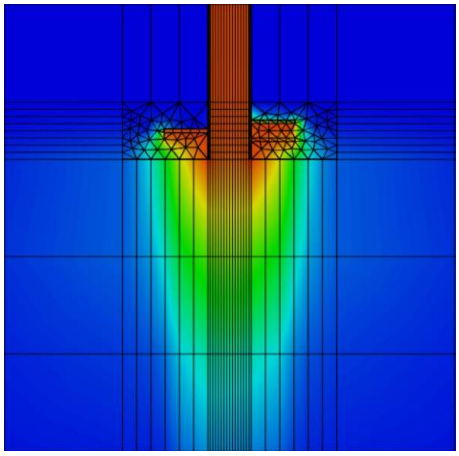

(b)

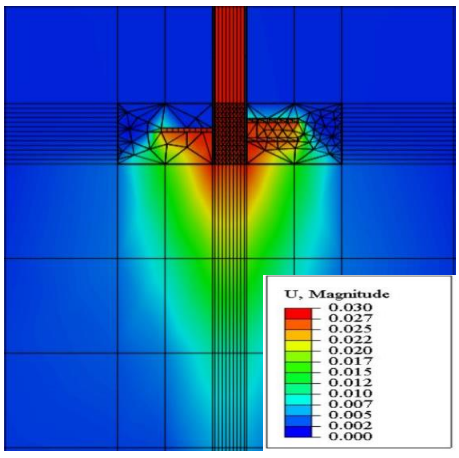

(c)

Fig. 10 Vertical Displacement Contours of the single helical pile resting in medium sandy soil having different Dh/Ds ratios for 8m pile length: (a) Dh/Ds=2 (b) Dh/Ds=3 (c) Dh/Ds=4.

The compression capacity of helical pile for CSF can be calculated as:

$$P_{cylindrical} = 2D_h\gamma\,(Nq'-1)\,A_{end} + \beta[(H_e + (m-1)S/2\gamma K_h \tan\phi](m-1)S\pi D_h + f_s H_e(\pi d) \quad \text{(vi)}$$

The first term of Eq. (vi) calculates end bearing of the bottom helix. The second term of Eq. (vi) implies the shear force mobilized across the disturbed cylindrically shaped soil between the top and bottom plates. The third term of Eq. (vi) calculate the bearing due to shear force around the shaft.

m = 1; S = 0 m; H_e = 5.28 m

Hence,

$$P_{cylindrical} = 118.01+0+80.01 = 198 \text{ kN} \quad \text{(vii)}$$

Table 4 shows the comparison of the compression capacity of the helical pile obtained through numerical analysis in this study with the suggested analytical solutions for IBF and CSF of cohesion less soil.

Table 4 reveals that there is an insignificant difference between the numerical capacity and theoretical theories. For medium soil having 6

Table 4 The comparison of the compression capacity of the single helical pile with theories (Dh/DS = 2).

H (m)	Sand Type	Numerical Capacity (kN)	Theoretical Calculated Capacity (kN)	Percentage variation (%)
			Individual Bearing	
6	Loose	120	135.70	13.08%
	Medium	255	292.20	14.58%
	Dense	678	706.21	4.16%
8	Loose	185	202.26	9.32%
	Medium	410	422.72	3.10%
	Dense	950	1034.27	8.87%

m pile depth, the numerical capacity and theoretical capacity were 255 kN and 292.20 kN, respectively. The average deviation in numerical capacity was 8.85% corresponding to the theoretical capacity.

4.2. Compression capacity of multi-helical Pile in sand

4.2.1. The effect of soil parameters

The load-displacement curves of a helical pile resting in loose, medium, and dense sandy soil having inter-helix spacing ratio of 1.5 and Dh/Ds = 2, and pile depths of 6 m and 8 m are shown in Fig. 11 (a) and (b). Similar to a single helical pile, the compression capacity of double helical pile increases with the rise in the friction angle of the soil. For a helical pile depth of 6 m, S/D_h = 1.5 and D_h/D_S = 2, the obtained compression capacity for ϕ= 25°, 33°, and 40° were 177.47 kN, 395.16 kN, and 988.17 kN, respectively. Likewise, for a helical pile depth of 8 m, the compression capacity values were 265.47 kN, 602.49 kN and 1461.49 kN, respectively.

4.2.2. The effect of Pile depth (H)

Fig. 12 depicts the load-displacement curves of double helical piles with lengths of 6 m and 8 m, having S/D_h = 1.5, and D_h/D_S = 3. An increment in the compression capacity of the helical pile was observed with a rise in the pile depth. For medium sandy soil at S/D_h = 1.5 and D_h/D_S = 3, the load capacities obtained for 6 m and 8 m pile depths were 379.37 kN and 352.89 kN, respectively. The observed behavior may be attributed to the rise in frictional resistance between the helical shaft and surrounding soil with the increase in pile depth which mobilizes the shear forces.

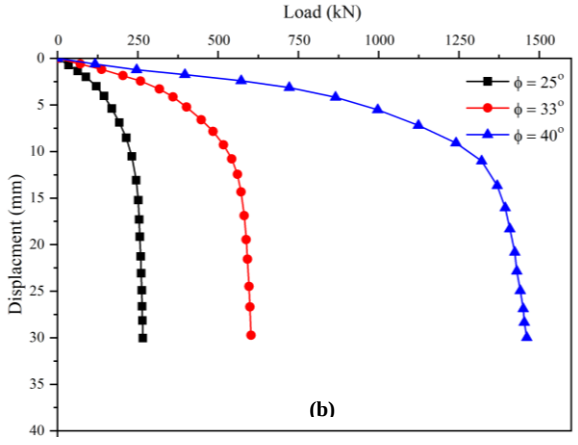

Fig. 11 Load-displacement curves of the double helical pile resting in loose, medium, and dense sandy soil having (a) 6 m and (b) 8m pile depths (Dh/DS = 2 and S/Dh = 1.5).

4.2.3. The effect of Dh/DS on the compression capacity

Fig. 13 (a) & (b) shows the load-displacement curves of 6 m and 8 m long helical pile with S/Dh = 2 for different D_h/D_S ratios resting in medium sandy soil. The load-displacement curves showed the same behavior as that observed for single helical pile. As the shaft diameter was increased, the load-displacement curves of the piles increased sharply. For instance, at S/D_h =1.5 and D_h/D_S = 2 for a pile depth of 6 m, the compression capacity was 395.16 kN which reduced to 379.37 kN, and 352.89 kN for D_h/D_S = 3 and 4, respectively. Similarly, for 8 m pile length the compression capacity was 602.49 kN at D_h/D_S = 2 which declined to 527.19 kN and 479.46 kN for D_h/D_S = 3 and 4, respectively. As the diameter of the shaft increases, interaction between the surrounding soil and helical pile increases which may have led to these observations.

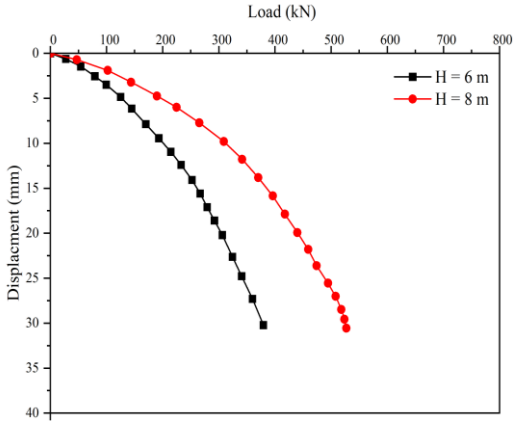

Fig. 12. Load-displacement curves of the double helical pile resting in medium sandy soil for different pile depths (S/Dh = 1.5 and Dh /DS = 3).

4.2.4. The effect of Inter-helical spacing ratio (S/Dh)

The inter-helical spacing of multiple helical pile significantly influences the compression capacity. The CSF and IBF depends upon the inter-helix spacing. Nowkandeh and Choobbasti [13] documented that up to a certain limit, change in the S/D_h ratio influences the compression capacity of a helical pile. The load-displacement curves of 6 m and 8 m pile depths resting in medium sandy soil at D_h/D_S = 2, and S/D_h = 1.5, 2 and 3 are shown in Fig. 14 (a) and (b), respectively. The study of Figs. 14 (a) and (b) reveals that for various S/DH ratios, the load deformation curves initially had a linearly elastic slope. This indicates that at smaller displacements, the inter-helix spacing ratio does not have considerable influence on the compression capacity. The failure of the helical pile was governed by individual bearing failure [19].

With an increase in the S/D_h ratio, the compression capacity increases. For instance, the compression capacity of a helical pile (H = 6 m and D_h/D_S = 4) resting in medium sandy soil at S/D_h = 1.5 was 352.89 kN which increased to 378.44 kN and 465.76 kN at S/D_h = 2 and 3, respectively. Cylindrical shear failure was observed at S/D_h = 1.5 and 2 (as shown Fig. 15 (a) and (b)). Whereas, the individual bearing failure mode was observed at a higher S/D_h (S/D_h = 3). Due to the individual bearing failure soil movement became more concentrated toward the individual helix, ultimately leading to an increase in the compression capacity. Perko and Wiley [17] reported that the optimum spacing ratio should be at a point where the failure modes changes from CSF to IBF.

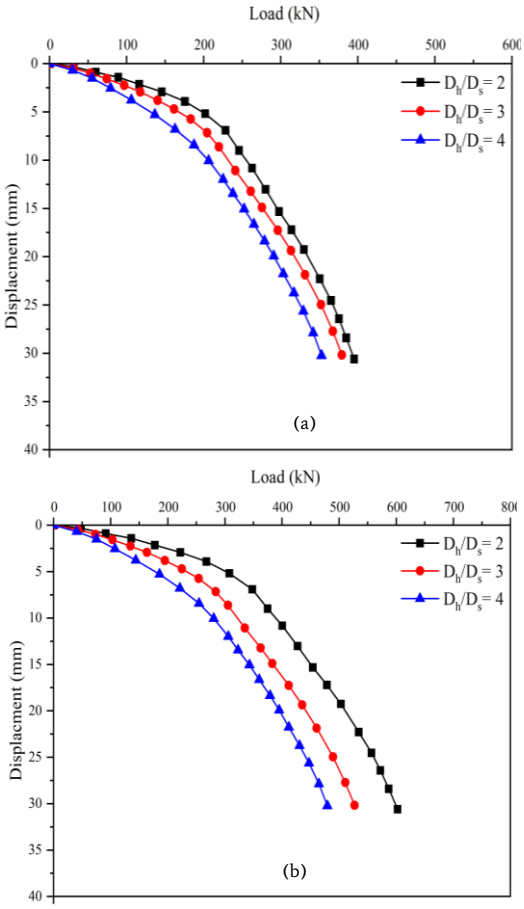

Fig. 13 Load-displacement curves of the double helical pile resting in medium sandy soil for different Dh/Ds ratios (a) 6 m pile depth (b) 8 m pile depth (S/Dh =1.5).

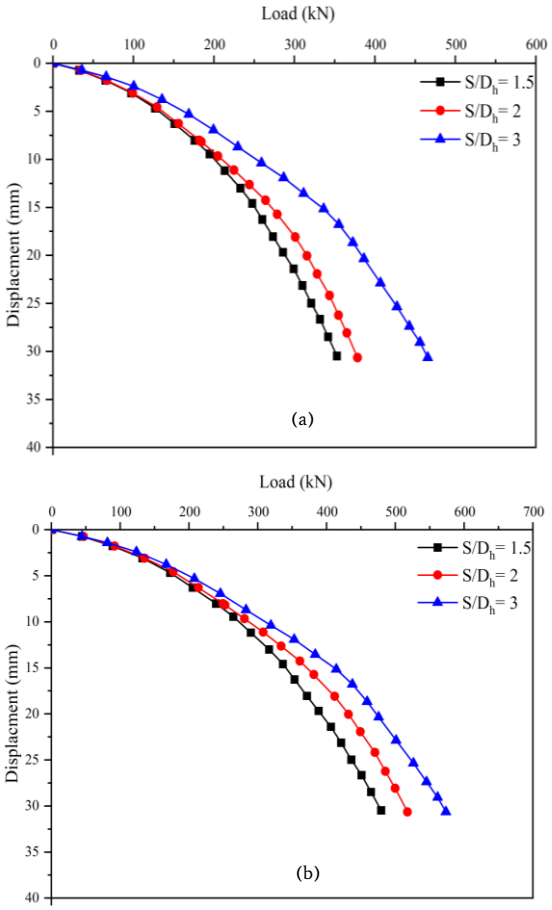

Fig. 14 Load-displacement curves of the double helical pile resting in medium sandy soil for different for various inter-helix spacing ratios at Dh/DS = 4 (a) 6 m; (b) 8m lengths.

In this study, the change in the failure mode was observed at S/D_h = 3, where each helix failed individually without affecting the other helices (Fig. 15 (c)).

4.2.5 Displacement contour

The vertical displacement contours of a helical pile resting in medium sand having inter-helix spacing ratios of 1.5, 2 and 3 and pile depth of 6m and 8m at D_h/D_s = 4 for double helical pile are shown in Figs. 15 and 16, respectively. The displacement was limited to pile tip and helix. Contrary to this, Nowkandeh and Choobbasti [13] found that for short helical piles with a depth 4 m, the displacement contours enclosed a cylinder around the helix and extended to the ground surface. This discrepancy could be because of the idealization of the circular disk. A clear change in the mechanism from CSF to IBF of the double helical pile with an increase in S/D_h ratio can be seen in Figs. 15 and 16. Figs. 15 (a) and (c) reveal a cylindrical shear failure at S/D_h = 1.5 which changed to individual bearing failure at S/D_h = 3. The transition state of the double helical pile occurred at S/D_h = 2 as shown in Fig. 15 (b).

4.2.6. Theoretical Capacity for Double helical pile

The pile compression capacity of a multi-helical pile in sandy soil is calculated by Eqs. (i) and (vi). For medium dense sand, the compression capacity based on the IBF can be calculated as:

ϕ = 33°; D_h = 0.61 m; γ = 18 kN/m^3; N_q' = 27.13; A_n = 0.22 m^2; A_{end} = 0.22 m^2; n = 1; H = 6 m; d = 0.31 m; K_h = 1.26; f_S = 29.19

$P_{individual}$ = 540.95 kN

The compression capacity based on the CSF for a multi-helix pile can be calculated as:

m = 1; S = 0.915 m; H_e = 4.965 m

Hence, $P_{cylindrical}$ = 355.76 kN

Table 5 demonstrates the comparison of the compression capacity of a double helical pile obtained through numerical analysis with the suggested analytical solution. The numerical compression capacity obtained from the analysis was lower than the theoretical values. For instance, for the compression capacity of a helical pile (H = 6 m, D_h/D_s = 2 and S/D_h = 1.5) resting in medium sandy soil, the variation in numerical and theoretical compression capacities was 14%. Similarly, at the same instance for 8 m pile depth, the variation was 16%. This discrepancy may be due to Eqs. (i) and (vi) assuming the soil shear stress around the helix and the pile shaft was fully mobilized. However, in this study the displacement of 30 mm was given which might have been insufficient to cause complete failure of the pile.

4.3. The effect of number of helices

In this section, a comparison between the compression capacity obtained for single and double helical piles with length of 6 m at S/D_h = 1.5, resting in loose, medium, and dense sandy soil has been discussed. Fig. 17 demonstrates the effect of variations in the friction angle and D_h/D_s ratio on the compression capacity of single and double helical piles. It can be depicted from Fig. 17 that the compression capacity of a double helical pile is more than that of a single helical pile at specific values of ϕ and D_h/D_s ratio. For example, at ϕ = 33° and D_h/D_s = 3, the compression capacity of a single helical pile was 252.64 kN which increased to 403.96 kN for a double helical pile. This increase in the

Table 5. The comparison of the compression capacity of the double helical pile with theories (Dh/DS = 2 and S/Dh = 1.5).

H (m)	Sand Type	Numerical Capacity (kN)	Theoretical Capacity (kN)		Percentage variation (%)	
			Individual Bearing	Cylindrical Bearing	Individual Bearing	Cylindrical Bearing
6	Loose	177.47	208.00	152.08	15.84	15.41
	Medium	395.16	538.42	355.76	30.69	10.49
	Dense	988.17	1272.66	865.98	25.17	13.18
8	Loose	265.47	268.59	225.19	1.17	16.42
	Medium	602.49	680.18	510.76	12.11	16.48
	Dense	1461.49	1609.25	1255.54	9.62	15.16

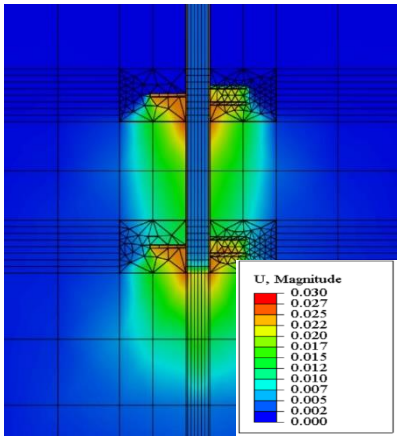

(a)

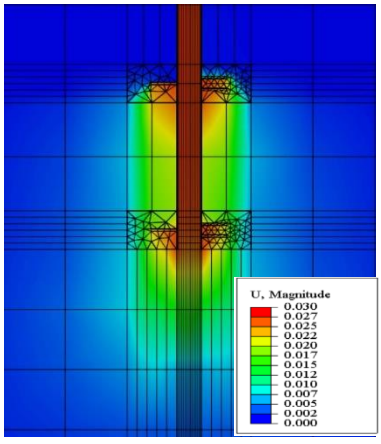

(b)

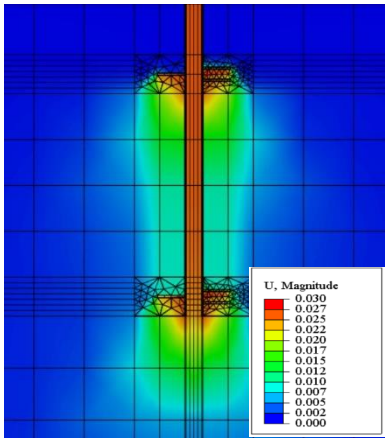

(c)

Fig. 15 Vertical displacement contours for the double-helical Pile having pile length 6m in medium sandy soil: (a) S/Dh=1.5 (b) S/Dh =2 (c) S/Dh =3.

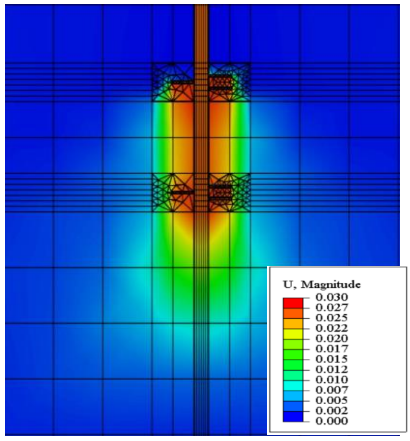

(a)

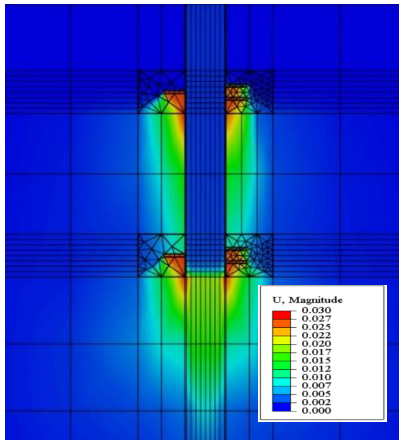

(b)

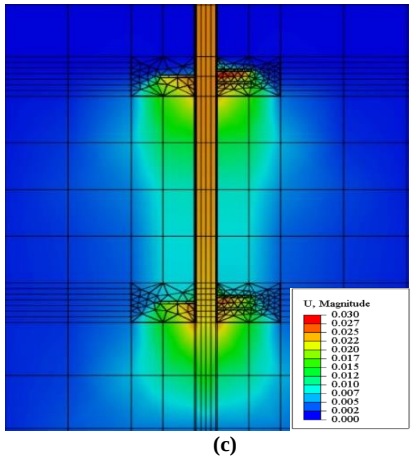

(c)

Fig. 16 Vertical displacement contours for the multi-helical Pile having pile length 8m in medium sandy soil: (a) S/Dh=1.5 (b) S/Dh =2 (c) S/Dh =3.

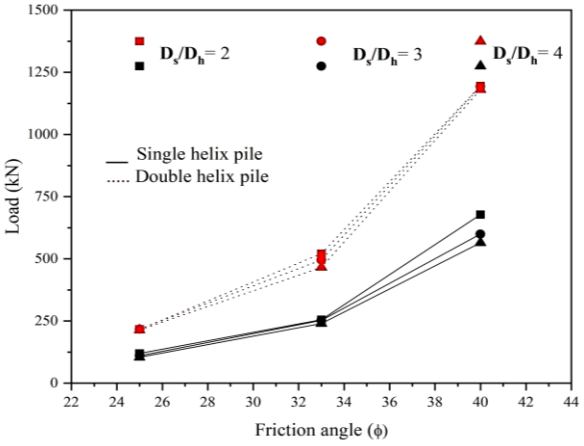

Fig. 17 The comparison of the bearing capacity of the single and double helical pile.

compression capacity may be due to an increase in end bearing.

4.4. The comparison of the compression capacity with conventional concrete pile

A dimensionless number (I), defined as the ratio of the compression capacity of a helical pile (Q_{helix}) to that of a concrete pile ($Q_{concrte}$) with the same depth and diameter, was calculated. Table 6 summarizes the $Q_{helix}/Q_{concrete}$ ratio of pile resting in medium sand. In the case of conventional concrete pile, the compression capacity decreases sharply with a decrease in the diameter of shaft, However, for helical pile, the rate of reduction in the compression capacity with the diameter of shaft is less. For example, for medium soil of 6 m pile depth and diameters of 0.305 m, 0.203 m, and 0.152 m, the compression capacity attained for single helical and concrete pile were 255 kN, 252.65 kN, and 239.88 kN, and 410 kN, 346.92 kN and 305.14 kN, respectively. The corresponding 'I' values were 1.16, 3.19, and 6.08, respectively. The compression capacity is directly proportional to the diameter of the helical plate which provides additional resistance. Thus, the compression capacity of the helical pile was more than that of the conventional concrete pile.

Table 1 $Q_{helical}/Q_{concrete}$ ratio of the pile resting in medium sand.

H (m)	D_s	$Q_{helical}$	$Q_{concrete}$	$Q_{helix}/Q_{concrete}$ (I)	Percentage Increase (%)
6	0.305	255	218.40	1.16	17%
	0.203	252.65	79.11	3.19	219%
	0.152	239.88	39.41	6.08	509%
8	0.305	410	251.53	1.63	63%
	0.203	346.92	93.79	3.69	270%
	0.152	305.14	47.64	6.40	540%

4.5. The comparison of the compression capacity with Single Under-reamed pile

A dimensionless number (R), defined as the ratio of the compression capacity of a single helical pile (Q_{helix}) to that of a single under-reamed pile ($Q_{under\text{-}reamed}$) with the same depth and diameter, was calculated. Table 7 summarizes the $Q_{helix}/Q_{under\text{-}reamed}$ ratio of pile resting in dense sand. The compression capacity of the helical pile with a single helix is the same as the compression capacity of a single under-reamed pile. For example, for dense soil with a 6 m pile depth and D_h/D_s = 2, 3 and 4, the compression capacity attained for the single helical and single under-reamed were 678 kN, 599.73 kN, and 564.97 kN and 659.83 kN, 589.46 kN and 552.2 kN, respectively. The corresponding 'R' values were 1.028, 1.017 and 1.023, respectively, whereas, the compression capacity of a single under reamed pile in the case of loose and medium sandy soil was more than that of the single helical pile.

Table 7. Qhelical/Qunder-reamed ratio (Single) of the pile resting in dense sand.

H (m)	D_h/D_s	Q_{Single} (Helical Pile)	Q_{Single} (under-reamed)	$Q_{helix}/Q_{under\ reamed}$ (R)	Percentage Increase (%)
6	2	678	659.83	1.028	3%
	3	599.73	589.46	1.017	2%
	4	564.97	552.2	1.023	2%
8	2	950	894.28	1.062	6%
	3	837.14	743.67	1.126	13%
	4	725.53	667.08	1.088	9%

4.6. The comparison of the compression capacity with Double Under-reamed pile

A dimensionless number (J), defined as the ratio of the compression capacity of double helical pile (Q_{helix}) to that of a double under-reamed pile ($Q_{under\text{-}reamed}$) with the same depth and diameter, was calculated. Table 8 summarizes the $Q_{helix}/ Q_{under\text{-}reamed}$ ratio of pile resting in dense sand. The compression capacity of the double helical pile was greater than that of the double under-reamed pile. For example, for dense soil with a 6 m pile depth and D_h/D_s = 2, 3 and 4, the compression capacity attained for the double helical and double under-reamed pile were 1195.61 kN, 1193.36 kN, and 1180.61 kN and 1581.49 kN, 1451.49 kN and 1324.71 kN, respectively. The corresponding 'I' values were 1.028, 1.017 and 1.023, respectively. At S/D_h = 3, the failure of a double helical pile changes from CSF to IBF, whereas for the under-reamed pile, the shear failure pattern remains cylindrical. The compression capacity of the double under-reamed pile in the case of loose and medium sandy soil was more than that of the single helical pile.

5. Conclusions

A numerical investigation was conducted to calculate the load capacity of helical pile resting in sandy soil subjected to compressive load using ABAQUS. The conclusions drawn are as follows:

- For single helical pile, the compressive capacity increases with an increase in the pile depth and friction angle of sand. However, the compression capacity decreases with an increment in D_h/D_S.
- Similarly, for double helical pile, the compression load increase with the rise in the friction angle and pile depth, and decreases with the increase in D_h/D_S ratio.
- Continuous increment in the compression capacity is seen for a double helical pile with the increase in S/Dh ratio. For a better performance, the S/D_h can be taken as 3, because at this value the performance in governed by individual bearing failure.
- The helical pile exhibits a higher compression load carrying capacity in comparison to conventional concrete pile of equal length and diameter resting in different sandy soils.
- For dense sand, the single helical pile has shown a similar compression capacity to that of a single under-reamed pile of the same dimensions. However, when compared to a single under-reamed pile resting in loose and medium sandy soil, the compression load of the single helical pile is lower
- The comparison between the compressive capacity of a double helical pile and a double under-reamed pile of the same dimensions show that the the double helical pile performs better in dense sand. However, in loose as well as medium sandy soil, the performance of the double under-reamed pile is better than that of the double helical pile, because of the cylindrical shear failure of the under-reamed pile.

REFERENCES

[1] Rao SN, Prasad YVSN, Shetty MD (1991) Behaviour of model screw piles in cohesive soils. SOILS Found Vol 31:.

https://doi.org/10.1016/0148-9062(92)92490-4

[2] Rao SN, Prasad YVSN, Veeresh C (1993) Behaviour of embedded model screw anchors in soft clays. Geotechnique 43:605–614. https://doi.org/10.1680/geot.1993.43.4.605

[3] Livneh B, El Naggar MH (2008) Axial testing and numerical modeling of square shaft helical piles under compressive and tensile loading. Can Geotech J 45:1142–1155. https://doi.org/10.1139/T08-044

[4] Elsherbiny ZH, El Naggar MH (2013) Axial compressive capacity of helical piles from field tests and numerical study. Can Geotech J 50:1191–1203. https://doi.org/10.1139/cgj-2012-0487

[5] Lutenegger AJ (2009) Cylindrical Shear or Plate Bearing? — Uplift Behavior of Multi-Helix Screw Anchors in Clay. 456–463. https://doi.org/10.1061/41021(335)57

[6] Sprince A, Pakrastinsh L (2010) Helical pile behaviour and load transfer mechanism in different soils. 10th Int Conf Mod Build Mater Struct Tech 1174–1180

[7] Lutenegger AJ (2011) Behavior of Multi-Helix Screw Anchors in Sand. Proc 14thPan-American Conf Soil Mech Geotech Eng Pap No 126

[8] Nabizadeh F, Choobbasti AJ (2017) Field Study of Capacity Helical Piles in Sand and Silty Clay. Transp Infrastruct Geotechnol 4:3–17. https://doi.org/10.1007/s40515-016-0036-0

[9] Salhi L, Nait-Rabah O, Deyrat C, Roos C (2013) Numerical modeling of single helical pile behavior under compressive loading in sand. Electron J Geotech Eng 18 T:4319–4338

[10] Knappett JA, Brown MJ, Brennan AJ, Hamilton L (2014) Optimising the Compressive Behavior of Screw Piles in Sand for

[11] Sırsıkar RA (2018) ++Study of Helical Pile Behaviour in Cohesionless Soil (bu makaleyle artık işim yok). 1–41

[12] George BE, Banerjee S, Gandhi SR (2020) Numerical analysis of helical piles in cohesionless soil. Int J Geotech Eng 14:361–375. https://doi.org/10.1080/19386362.2017.1419912

[13] Nowkandeh MJ, Choobbasti AJ (2021) Numerical study of single helical piles and helical pile groups under compressive loading in cohesive and cohesionless soils. Bull Eng Geol Environ 80:4001–4023. https://doi.org/10.1007/s10064-021-02158-w

[14] Angurana DI, Yadav JS, Khatri VNK (2023) Estimation of Uplift Capacity of Helical Pile Resting in Cohesionless Soil. Transp Infrastruct Geotechnol. https://doi.org/10.1007/s40515-023-00299-x

[15] Jahanshahi Nowkandeh M, Ashtiani M (2023) Cushioned helical-piled raft systems to mitigate hazards associated with normal faulting. Soil Dyn Earthq Eng 166:107773. https://doi.org/10.1016/j.soildyn.2023.107773

[16] Mehrabani A, Heidarzadeh H, Kamgar R (2022) Monitoring and estimating pull-out force produced by inclined-micropile groups with various characteristics. Arab J Geosci 15:. https://doi.org/10.1007/s12517-022-09541-1

[17] Rasoul Alipour, Hesam Aminpour AD 3 (2023) Investigating the effect of soil improvement by micropile method in marl soil: a case study of Bidboland, Khuzestan. Amirkabir J Civ Eng 54:4573–4588. https://doi.org/10.22060/ceej.2022.20705.7506

[18] Szypcio Z, Dołżyk k (2006) The bearing capacity of layered subsoil. Stud Geotech Mech XXVIII/1 1:2006

[19] Stas C, Kulhawy F (1984) Critical evaluation of design methods for foundation under axial uplift and compression loading. Final Rep No EPRI-EL-3771 Ithaca, NY Cornell Univ

[20] Perko HA, Wiley J (2009) Helical Piles

[21] Mitsch M, Clemence S (1985) The uplift capacity ofhelix anchors in sand. Uplift Behav ofAnchor Found Soil Am Soc ofCivil Eng New York, NY, pp 26–47 Oct 24